Microscopic mechanisms for improper ferroelectricity in multiferroic perovskites: a theoretical review

Microscopic mechanisms for improper ferroelectricity in multiferroic perovskites: a theoretical review

**Silvia Picozzi[1], Kunihiko Yamauchi[1], Ivan A Sergienko[2,3],
Cengiz Sen[2,3,5], Biplab Sanyal[4] and Elbio Dagotto[2,3]**

[1] CNR-INFM, CASTI Regional Laboratori c/o Dipartimento di Fisica, Università degli Studi dell'Aquila, 67100 Coppito (L'Aquila), Italy

[2] Materials Science and Technology Division, Oak Ridge National Laboratory, Oak Ridge, TN 37831, USA

[3] Department of Physics, The University of Tennessee, Knoxville, TN 37996, USA

[4] Theoretical Magnetism Group, Department of Physics, Uppsala University, Box-530, SE-75121, Sweden

E-mail: silvia.picozzi@aquila.infn.it

Abstract

Two microscopic mechanisms helping us to understand the multiferroic behavior of distorted rare-earth manganites are here briefly reviewed. The original work was carried out by means of Hamiltonian modeling and first-principles density functional simulations. Our first topic concerns the link between the Dzyaloshinskii–Moriya interaction and ferroelectricity in incommensurate magnets. We argue that the Dzyaloshinskii–Moriya interaction may play a key role since (i) it induces ferroelectric displacements of oxygen atoms and (ii) it favors the stabilization of a helical magnetic structure at low temperatures. Our second topic concerns the prediction, based on Landau theory, that the symmetry of the zigzag spin chains in the AFM-E (E-type antiferromagnetic) orthorhombic manganites (such as $HoMnO_3$) allows a finite polarization along the c axis. The microscopic mechanism at the basis of ferroelectricity is interpreted through a gain in band energy of the e_g electrons within the orbitally degenerate double-exchange model. Related Monte Carlo simulations have confirmed that the polarization can be much higher than what is observed in spiral magnetic phases. Density functional calculations performed on orthorhombic $HoMnO_3$ quantitatively confirm a magnetically induced ferroelectric polarization up to ~ 6 μC cm^{-2}, the largest reported so far for improper magnetic ferroelectrics. We find in $HoMnO_3$, in addition to the conventional displacement mechanism, a sizable contribution arising from the purely electronic effect of orbital polarization. The relatively large ferroelectric polarization, present even with centrosymmetric atomic positions, is a clear sign of a magnetism-induced electronic mechanism at play, which is also confirmed by the large displacements of the Wannier function centers with respect to the corresponding ions in AFM-E $HoMnO_3$. The final polarization is shown to be the result of competing effects, as shown by the opposite signs of the e_g and t_{2g} contributions to the ferroelectric polarization.

(Some figures in this article are in colour only in the electronic version)

1. Introduction

Multiferroics (MFs) are materials that show at the same time spontaneous ferroelectric and magnetic orders. Magneto-electrics are materials where a magnetic (electric) field can induce an electric (magnetic) polarization. These are classes of materials particularly attractive for future technologies, since the interplay between magnetism and ferroelectricity could be exploited, aiming at a new generation of electrically controlled spintronic devices [1, 2].

[5] Present address: Department of Physics, University of Cincinnati, OH 45221, USA.
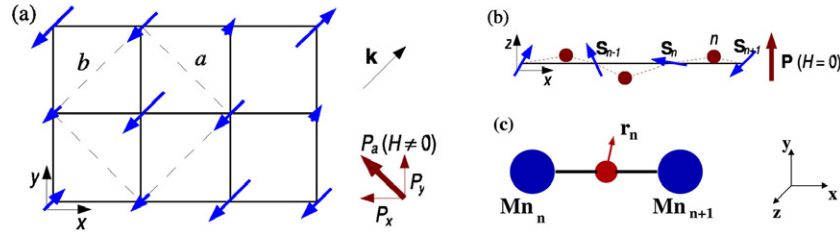
Figure 1. ((a), (b)) Sketch of the ground state structure of TbMnO$_3$, reproduced from [14]. (a) Projection of the Mn spins onto the xy plane. Dashed lines are the boundaries of the unit cell in the orthorhombic setting. The diagram on the right illustrates the emergence of the in-plane component of P in an applied magnetic field. (b) The zx projection of the spin structure and positions occupied by the O ions (filled circles). (c) The Mn$_2$O 'molecule' in the cubic perovskite structure. The vector $\mathbf{r}_n$ denotes the displacement of the O ion.

In this paper, we will mainly focus on MFs showing *improper* ferroelectric (FE) order, i.e. when ferroelectricity occurs as a *secondary* effect or concomitantly with some other kind of ordering (such as spin ordering, in particular). This is at variance with the case for proper conventional FEs (such as BaTiO$_3$) where the structural instability towards the polar state is the main driving force behind the phase transition. Being a by-product and not a driving force, ferroelectricity often appears as a weak phenomenon in MFs. In fact, the order of magnitude for the FE polarization P is typically 0.1 μm^2 in experimentally studied improper magnetic FEs (IMF) [3, 4]. However, it is within this class of materials that the two ordering phenomena appear at the same time, raising the expectation that a strong coupling between magnetism and ferroelectricity should exist. Initially motivated by possible practical applications such as magnetically controlled non-volatile FE memory [5, 6], the field has unveiled an extremely rich and fascinating fundamental condensed matter physics problem. This has motivated a flurry of activity, especially as regards the prototypical multiferroic manganites RMnO$_3$ (R being a rare-earth element). This class of compounds will be the focus of the present brief theoretical review, which shows the results of a joint Hamiltonian modeling/density functional study. Hamiltonian modeling is key to proposing microscopic mechanisms at the basis of the multiferroic behavior in manganites (see section 2.1 for the magnetically incommensurate phase and section 2.2 for the collinear AFM-E phase). In parallel, first-principles calculations based on density functional theory (DFT) appear to be well suited to addressing some of the critical issues that are not easily accessible through experiments, such as the value of P (see section 3.2) and the structural and electronic mechanisms of ferroelectricity (see section 3.3).

According to [5, 7, 8], in RMnO$_3$ (R = Tb, Dy) the ground state is at the same time magnetically incommensurate (ICM, i.e. with a magnetic order which is not commensurate with the lattice period) and FE, with the FE polarization **P** directed out of the ab plane (*Pbnm* setting). The magnetic propagation vector **k** is directed along the b axis within the xy plane, and the out-of-plane coupling is AFM. A neutron diffraction study suggested that, for temperatures $T < 28$ K [3], the classical low temperature spin structure of the Mn sublattice in TbMnO$_3$

can be described as[6]

$$S_n^i = S_0^i \cos(n\theta + \alpha_i), \qquad (1)$$

where $i = x, y, z$, $S_0^x = S_0^y \approx S_0^z = 1.4$, $\theta = 0.28\pi$, and n enumerates the Mn ions along a chain in the x direction (see figure 1(b)). According to [3], $\alpha_x = \alpha_y$, whereas the experiment was insensitive to the difference between α_x and α_z. In parallel, the lattice structure was also shown to be IC with the modulation vector $\mathbf{k}_l = 2\mathbf{k}$ [5]. For 28 K $< T <$ 41 K, another incommensurate, collinear magnetic structure is found without any detected ferroelectricity [5, 3].

On a related topic, the antiferromagnetic (AFM) E-type phase of manganites is characterized by in-plane zigzag ferromagnetic (FM) chains antiferromagnetically coupled to neighboring chains (see figure 5(a) reported below); the out-of-plane coupling is AFM as well. This peculiar spin ordering is observed in orthorhombic HoMnO$_3$ [9] and its stabilization (proposed by means of a modeling study [10] and confirmed from *ab initio* approaches [11]) is due to the strong octahedral tilting (the Mn–O–Mn angle is as small as ∼144° in HoMnO$_3$). The reason why this phase is mentioned in this study is that a multiferroic behavior was recently experimentally observed in ortho-HoMnO$_3$ [12] after theoretical studies predicted the existence [13]. These studies are reviewed here. It is important to remark that the mechanism and the value of the polarization ($<$0.1 μC cm^{-2}) are still under debate (see below) and the detailed analysis of the multiferroic properties of HoMnO$_3$ calls for further studies.

2. Predictions from Hamiltonian modeling

In this section, we will briefly review the main results obtained in [14, 13], using model Hamiltonians and a variety of analytical and numerical techniques. It is important to remark that this study is not intended to be a comprehensive review of this field of research. As a consequence, readers should search not only for additional details about the calculations but also for proper citations to related literature in the two original publications [14, 13] discussed here.

---

[6] Here, we do not consider the magnetic moments of the rare-earth ions explicitly, since they are not directly related to the FE order.

2.1. Dzyaloshinskii–Moriya interaction in multiferroic perovskites

Trying to understand the link between atomic displacements and spin interactions, let us first examine the case of an isotropic superexchange. Let us assume the Mn ions to be fixed in their original locations, while the O ions can displace with respect to their paraelectric (PE) positions. We will consider a chain of Mn ions in the x direction, for simplicity to guide the intuition. We denote with $\mathbf{r}_n = (x_n, y_n, z_n)$ the displacement of the O ion located between the Mn spins $\mathbf{S}_n$ and $\mathbf{S}_{n+1}$ from its position in the ideal cubic perovskite structure. There, the Mn$_2$O 'molecule' subset shown in figure 1(c) has inversion symmetry. Since the symmetric superexchange ($\mathbf{S}_n \cdot \mathbf{S}_{n+1}$) is invariant under inversion (i.e. the bare interchange of $\mathbf{S}_n$ and $\mathbf{S}_{n+1}$), this coupling can only depend on even powers of $\mathbf{r}_n$. In the orthorhombically distorted structure, however, the oxygen atoms are displaced, so that $\mathbf{r}_n = (-1)^n \mathbf{r}_0 + \delta\mathbf{r}_n$, where $\mathbf{r}_0$ is constant (r_0 is typically a fraction of 1 Å) [15], and $\delta\mathbf{r}_n$ is the additional displacement, associated with the IC structure (the δr_n are of the order of 10^{-3} Å). It can be shown [14] that the model based on isotropic superexchange leads to

$$\delta z_n = (-1)^n \frac{J'_{\perp} z_0}{2\kappa} \sum_i S_0^{i2} \{\cos\theta + \cos[(2n+1)\theta + 2\alpha_i]\}, \quad (2)$$

where $J'_{\perp}$ represents an exchange constant and κ is the stiffness characterizing the elastic energy (similar expressions can be derived for δx_n and δy_n). Therefore, this model reproduces the observed structural modulation with the wavevector $2\mathbf{k}$ [5], but is insufficient to explain the net FE polarization, since $\sum_n \mathbf{r}_n = 0$ exactly.

However, let us now focus on the Dzyaloshinskii–Moriya interaction (DMI), i.e. an anisotropic exchange interaction [16, 17], where $\mathbf{S}_n \times \mathbf{S}_{n+1}$ changes its sign under inversion. Using group theory, the following expression can be shown to be invariant under *all* symmetry operations of the MnO$_2$ 'molecule' in the perovskite structure: $\mathbf{D}^{\mathbf{a}}(\mathbf{r}_n) \cdot [\mathbf{S}_n \times \mathbf{S}_{n+1}]$, where

$$\mathbf{D}^{\mathbf{x}}(\mathbf{r}_n) = \gamma(0, -z_n, y_n), \qquad \mathbf{D}^{\mathbf{y}}(\mathbf{r}_n) = \gamma(z_n, 0, -x_n) \quad (3)$$

for the Mn–O–Mn bonds along the x and y axes, respectively. For the Mn chain in the x direction, the portion of the Hamiltonian depending on $\delta\mathbf{r}_n$, namely

$$\delta H_{\mathrm{DM}} = \sum_n \mathbf{D}^{\mathbf{x}}(\delta\mathbf{r}_n) \cdot [\mathbf{S}_n \times \mathbf{S}_{n+1}] + H_{\mathrm{el}} \quad (4)$$

(H_{el} being the elastic energy), is minimized by

$$\delta z_n = \frac{\gamma}{\kappa} S_0^x S_0^z \sin\theta \sin(\alpha_x - \alpha_z), \quad (5)$$

and $\delta x_n = \delta y_n = 0$. The same result is obtained for the Mn chain in the y direction. Hence, the displacements in this model do not depend on n, leading to a net FE polarization along the z axis. Moreover, equation (4) shows that in the collinear spin structure experimentally observed for TbMnO$_3$, the equilibrium value of $\delta\mathbf{r}_n$ vanishes, leading to a PE state. Then, the DMI is a reasonable candidate for providing an understanding of the ferroelectric phase in manganites.

To further understand the role of the DMI in the stabilization of the ICM–FE phase, we considered [14] the Hamiltonian

$$\begin{aligned}
H = &-\sum_{\mathbf{i}a\alpha\beta\sigma} t_{\alpha\beta}^{\mathbf{a}} d_{\mathbf{i}\alpha\sigma}^{\dagger} d_{\mathbf{i}+\mathbf{a}\beta\sigma} - J_{\mathrm{H}} \sum_{\mathbf{i}} \mathbf{s}_{\mathbf{i}} \cdot \mathbf{S}_{\mathbf{i}} \\
&+ J_{\mathrm{AF}} \sum_{\mathbf{i}a} \mathbf{S}_{\mathbf{i}} \cdot \mathbf{S}_{\mathbf{i}+\mathbf{a}} + \sum_{\mathbf{i}a} \mathbf{D}^{\mathbf{a}}(\mathbf{r}) \cdot [\mathbf{S}_{\mathbf{i}} \times \mathbf{S}_{\mathbf{i}+\mathbf{a}}] \\
&+ \frac{\kappa_1}{2} \sum_{\mathbf{i}} (Q_{x\mathbf{i}}^2 + Q_{y\mathbf{i}}^2) + H_{\mathrm{JT}} + \frac{\kappa_2}{2} \sum_{\mathbf{i}} \sum_m Q_{m\mathbf{i}}^2, \quad (6)
\end{aligned}$$

based on the orbitally degenerate double-exchange model [18], for a two-dimensional square lattice, representing a MnO$_2$ layer, with periodic boundary conditions and one e_g electron per Mn^{3+} ion. Here $d_{\mathbf{i}\alpha\sigma}^{\dagger}$ is the creation operator for an electron on site $\mathbf{i}$, orbital $\alpha = x^2 - y^2$ (a) or $3z^2 - r^2$ (b), and carrying spin σ. The hopping integrals are given by $t_{aa}^{\mathbf{x}} = -\sqrt{3} t_{ab}^{\mathbf{x}} = -\sqrt{3} t_{ba}^{\mathbf{x}} = 3t_{bb}^{\mathbf{x}} \equiv t$ and $t_{aa}^{\mathbf{y}} = \sqrt{3} t_{ab}^{\mathbf{y}} = \sqrt{3} t_{ba}^{\mathbf{y}} = 3t_{bb}^{\mathbf{y}} = t$ (t is taken as the energy unit). J_{H} is the Hund's constant of coupling between the e_g electrons with spin $\mathbf{s}_{\mathbf{i}} = \sum_{\alpha\sigma\sigma'} d_{\mathbf{i}\alpha\sigma}^{\dagger} \sigma_{\sigma\sigma'} d_{\mathbf{i}\alpha\sigma'}$ (σ = Pauli matrices) and the three t_{2g} electrons are treated as a classical three-dimensional spin $\mathbf{S}_{\mathbf{i}}$. Hereafter, J_{H} is assumed to be infinite, which is a widely used approximation in the manganite context. $J_{\mathrm{AF}} > 0$ is the isotropic constant of superexchange between the t_{2g} spins. For simplicity, we consider DMI only between the t_{2g} spins and assume that the O ions are confined in the plane. $Q_{m\mathbf{i}}$ denotes the classical phonon coordinates associated with the displacements of the four O atoms surrounding the Mn site $\mathbf{i}$, with the doubly degenerate FE mode ($Q_{x\mathbf{i}}$ ($Q_{y\mathbf{i}}$)) representing a shift in the x (y) direction of the in-plane O atoms with respect to Mn. The Jahn–Teller (JT) interaction term is defined as usual [18, 19]. The remnant phonon modes (not FE or JT) are assumed to have the same spring constant κ_2 (an assumption that can be easily removed if needed). If $\kappa_1 = \kappa_2$, the ICM–FE phase is degenerate with other spin canted structures; therefore, we assume $\kappa_1 < \kappa_2$ to favor the ICM–FE phase.

Extensive Monte Carlo (MC) simulations of H have been performed, without taking into account the JT distortion (i.e. with $\lambda = 0$ in H_{JT}), on an 8×8 cluster, which is sufficiently large for our mainly qualitative purposes [14]. The low temperature ($T = 0.01$) results are presented in figure 2. For small γ, the J_{AF}–γ phase diagram shows the FM phase (which is the two-dimensional equivalent of the three-dimensional A-type antiferromagnetic phase)[7] and the E-type phase, in agreement with previous results [19]. Our most important result is that, for finite γ, a new modulated (ICM–FE) phase is stabilized. The presence of the three phases in the ground state phase diagram is in excellent agreement with experiments [5, 10]. The period of the ICM–FE phase is fixed in the MC simulations due to the small cluster used, but it is expected to vary smoothly with the parameters of H when the lattice size is increased, as discussed below. A typical snapshot showing the spin structure and O displacements in this phase

---

[7] We find that the FM phase is represented by two states, separated by the dotted line in figure 2(a). The regular FM phase with all spins aligned in the same direction is stable on the left-hand side of the dotted line, while the right-hand side is the domain of stability of the so-called 'twisted' phase with the period equal to the cluster length. This is a well-known effect of the finite cluster size and periodic boundary conditions [36, 37].
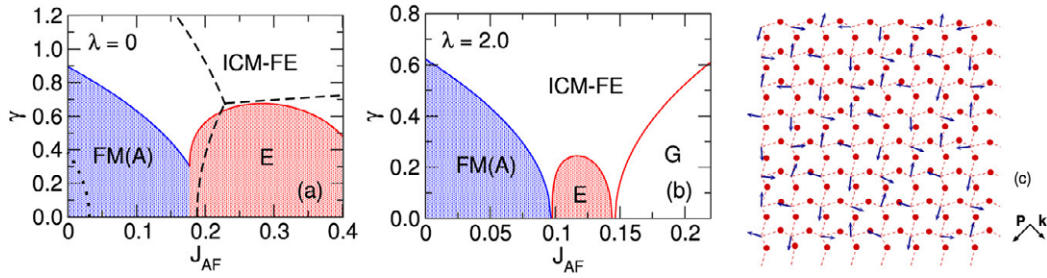
Figure 2. Low temperature results for model (6) with $\kappa_1 = 1$, $\kappa_2 = 10$, adapted from [14]. (a) Ground state phase diagram. The broken lines are Monte Carlo results for an 8×8 cluster. Solid lines are the results of calculations [14] in the thermodynamic limit. (b) Ground state phase diagram in the thermodynamic limit for the model with Jahn–Teller interaction (JTI). The JTI constant λ is defined in [19]. (c) Typical MC snapshot in the ICM–FE phase. Shown are the ICM modulation vector **k** and polarization P.
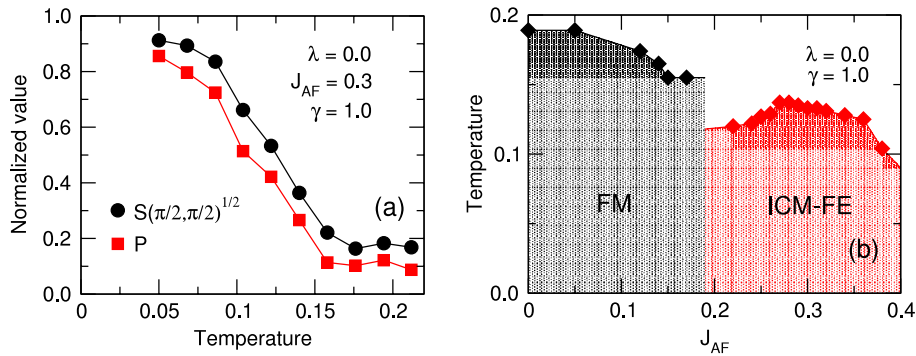

Figure 3. Finite temperature MC results for Hamiltonian H, using $\kappa_1 = 1$ and $\kappa_2 = 10$. (a) Typical temperature dependence of the ICM and FE order parameters. The order parameters are normalized to their maximum value at $T = 0$. (b) Temperature phase diagram. Results reproduced from [14].

is presented in figure 2(c) showing the spin modulation with wavevector $\mathbf{k} = (\pi/2, \pi/2)$. In the two-dimensional model studied here, the polarization **P** and the spins lie within the plane, as follows from confining the O ions to move within the plane. The ground state with **P** along the z direction can be obtained if model (6) is considered in three dimensions and the parameters of the model are modified to take into account the orthorhombic distortions of the cubic lattice.

To investigate the effects of the finite size on the ground state phase diagram, we calculated the energies for the ideal spin and phonon configurations, for which the e_g portion of H can be diagonalized exactly in the thermodynamic limit. This calculation becomes exact at zero temperature for the model considered here, with adiabatic phonons and classical spins, under the reasonable assumption that no other phases appear as ground states. In particular, we obtain for the ICM–FE phase,

$$E_{\text{ICM–FE}} = N \left(-1.60 \cos \frac{\theta}{2} + 2J_{\text{AF}} \cos \theta - \frac{\gamma^2}{4\kappa_1} \sin^2 \theta \right),$$
(7)

where N is the number of Mn sites in the lattice and θ is the angle between two nearest neighbor spins [14]. As shown in figure 2(a), while the boundary between the FM and E phases remains basically unchanged, the increase of the lattice size strongly affects the ICM–FE phase. This is reasonable, since θ can now assume the continuous values found by the minimization of (7), instead of being restricted by the boundary conditions of a small cluster. Generally, the absolute value of

k changes from zero at the FM–ICM phase transition to some finite value at the discontinuous ICM–E phase transition. Also, in the phase diagram obtained according to this procedure, only the regular FM–PE phase is found for small γ and $J_{\text{AF}} < 0.18$.

The minimal value of γ needed to stabilize the ICM–FE phase between A and E phases is calculated in the thermodynamic limit to be about 0.3 (see figure 2(a)), which corresponds to $\sim$200 meV Å^{-1} in the physical units, namely two orders of magnitude larger than the expected empirical value obtained above. However, these values can change as the model is improved. In particular, our zero-temperature results demonstrate that the minimal γ needed can be made infinitesimal if the JT interaction is taken into account. In figure 2(b) we show the results for a realistic value of $\lambda = 2.0$. In both cases ($\lambda = 0$ or 2), the calculated electronic density of states in the ICM–FE phase (not shown) has an insulating character, ensuring that the polarization is not screened out by the free charge carriers.

The results of the finite temperature MC study [14] are reproduced in figure 3. Figure 3(a) shows a typical temperature dependence of the ICM structure factor and absolute value of **P**. Within the simulation errors, the two order parameters show the same behavior and critical temperature, highlighting the strong mutual influence of ferroelectricity and magnetism. The corresponding temperature phase diagram is presented in figure 3(b).
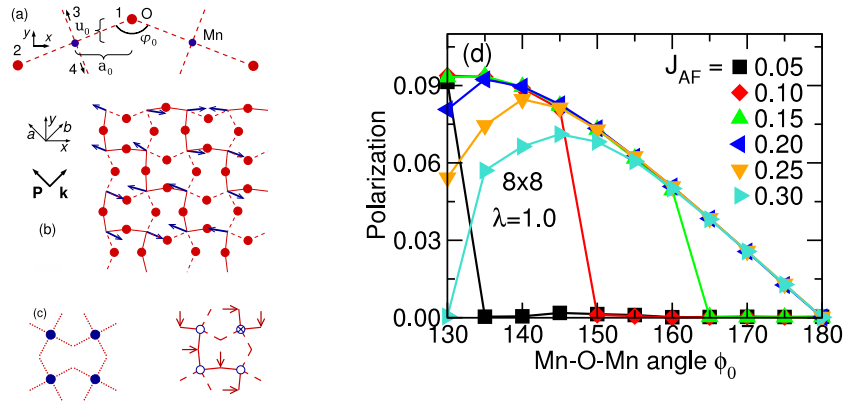
Figure 4. Results adapted from [13] to illustrate the presence of ferroelectricity in the *E* phase of manganites. (a) The starting configuration of a Mn–O–Mn bond. Numbers 1–4 enumerate the O atoms surrounding one Mn. (b) A MC snapshot of the improper magnetic ferroelectric E phase at $T = 0.01$. The ferromagnetic zigzag chain links are shown as solid lines. The displacements of the oxygen atoms are exaggerated. (c) Left: the local arrangement of the Mn–O bonds with disordered Mn spins (full circles). Right: oxygen displacements (arrows) within the chains of opposite Mn spins (open and crossed circles) in the *E* phase (see also [7, 4]). (d) MC results for the polarization at $T = 0.01$ for different values of J_{AF}.

2.2. Ferroelectricity in collinear spin configurations: the AFM-E phase

As explained in the introduction, recent theoretical and experimental results suggest that HoMnO$_3$ may have a net ferroelectric polarization. The magnetic order in this material is E, suggesting that it belongs to a different class compared with those that have a spin incommensurate order, where the DMI may contribute to the FE. As a consequence, in HoMnO$_3$ a new mechanism may be active. In [13], a possible scenario for ferroelectricity in this material was discussed, and here we briefly reproduce the main points of that discussion.

The AFM-E phase shows two different kinds of orientations, since it is formed by zigzag chains oriented at 45° with respect to the crystal axes. Let us denote these two orientations as E1 and E2 (see the left and right insets, respectively, of figure 6 reported below). They differ in the orientation of the central spins (i.e. parallel in E1 or antiparallel in E2 to the spin of the Mn atom at the origin). By means of the Landau theory of phase transitions, it can be shown [13] that the polarizations along the axes is $P_a = -c\chi(E_1^2 - E_2^2)$, $P_b = -d\chi(E_1^2 - E_2^2)E_1 E_2$, and $P_c = 0$, where χ is the dielectric susceptibility of the PE phase, and the other coefficients are phenomenological constants. Therefore, each of the four domains of the E phase [$(\pm E_1, 0)$ and $(0, \pm E_2)$] is IMF with the polarization along the a axis and different signs of P_a for E_1 and E_2.

The microscopic mechanism for ferroelectricity is investigated by means of Monte Carlo simulations using the following Hamiltonian for manganites based on the orbitally degenerate double-exchange model [18, 20, 19] with one e_g electron per Mn^{3+} ion:

$$H = -\sum_{\mathbf{ia}\alpha\beta} C_{\mathbf{i,i+a}} t_{\alpha\beta}^{\mathbf{ia}} d_{\mathbf{i}\alpha}^\dagger d_{\mathbf{i+a}\beta} + J_{AF} \sum_{\mathbf{ia}} \mathbf{S_i} \cdot \mathbf{S_{i+a}}$$
$$+ \lambda \sum_i (Q_{1\mathbf{i}}\rho_{\mathbf{i}} + Q_{2\mathbf{i}}\tau_{x\mathbf{i}} + Q_{3\mathbf{i}}\tau_{z\mathbf{i}}) + \tfrac{1}{2}\sum_{\mathbf{im}} \kappa_m Q_{m\mathbf{i}}^2, \quad (8)$$

where $\mathbf{S_i}$ is the classical spin of length 1, given by the polar angle $\theta_{\mathbf{i}}$ and azimuthal angle $\phi_{\mathbf{i}}$, representing the electrons occupying the t_{2g} orbitals on the $\mathbf{i}$th Mn site. $C_{\mathbf{i,j}} = \cos\frac{\theta_{\mathbf{i}}}{2}\cos\frac{\theta_{\mathbf{j}}}{2} + \sin\frac{\theta_{\mathbf{i}}}{2}\sin\frac{\theta_{\mathbf{j}}}{2}e^{-i(\phi_{\mathbf{i}}-\phi_{\mathbf{j}})}$ is the *double-exchange factor* arising due to the large Hund's coupling that projects out the e_g electrons with spin antiparallel to $\mathbf{S_i}$. $Q_{m\mathbf{i}}$ represent the classical adiabatic phonon modes, with stiffnesses κ_m, due to the displacements of the ligand oxygen ions surrounding the $\mathbf{i}$th Mn site. The phonon stiffnesses were chosen as follows— for the Jahn–Teller modes: $\kappa_1 = 2.0$, $\kappa_2 = \kappa_3 = 1.0$; for the FE mode: $\kappa_{FE} = 8.0$; and for the rest of the modes: $\kappa = 10.0$. The third term in equation (8) is the Jahn–Teller coupling with constant λ and the e_g orbital operators $\rho_{\mathbf{i}} = d_{\mathbf{i}a}^\dagger d_{\mathbf{i}a} + d_{\mathbf{i}b}^\dagger d_{\mathbf{i}b}$, $\tau_{x\mathbf{i}} = d_{\mathbf{i}a}^\dagger d_{\mathbf{i}b} + d_{\mathbf{i}b}^\dagger d_{\mathbf{i}a}$ and $\tau_{z\mathbf{i}} = d_{\mathbf{i}a}^\dagger d_{\mathbf{i}a} - d_{\mathbf{i}b}^\dagger d_{\mathbf{i}b}$.

To adapt it to the possibility of FE order, the model was improved over previous approaches as follows [13]. (i) The hopping parameters $t_{\alpha\beta}^{\mathbf{ia}}$ explicitly depend on the Mn–O–Mn angle $\varphi_{\mathbf{ia}}$. Considering only the largest Mn–O σ bond contribution, it was found [21] that $t_{aa}^{\mathbf{x}} = t_{aa}^{\mathbf{y}} = -t\cos^3\varphi$, $t_{bb}^{\mathbf{x}} = t_{bb}^{\mathbf{y}} = -t\cos\varphi/3$, $t_{ab}^{\mathbf{x}} = t_{ba}^{\mathbf{x}} = -t_{ab}^{\mathbf{y}} = -t_{ba}^{\mathbf{y}} = -t\cos^2\varphi/\sqrt{3}$, where $t = \frac{3}{4}(pd\sigma)^2$ is taken as the unit of energy. We neglect the φ dependence of J_{AF} since it has a smaller energy scale than t. (ii) The $Q_{m\mathbf{i}}$ are defined such that the elastic energy term in (8) is minimal for $\varphi_{\mathbf{ia}} \equiv \varphi_0 < 180°$. This is done in order to model the initial octahedral tilting (GdFeO$_3$ type) typical of orthorhombic perovskites [10]. In particular, the buckling mode is defined in two dimensions as $Q_{\text{buckle},\mathbf{i}} = y_{\mathbf{i}1} - y_{\mathbf{i}2} - x_{\mathbf{i}3} + x_{\mathbf{i}4} - (-1)^{i_x+i_y}4u_0$, where $x_{\mathbf{i}k}$, $y_{\mathbf{i}k}$ are the displacements of the oxygen atoms from their ideal positions in the 180° Mn–O–Mn bond, $u_0 = a_0\cot\frac{\varphi_0}{2}$, and a_0 is the Mn–O distance in the 180° Mn–O–Mn bond (see figure 4(a)). φ_0 is considered as a fixed parameter of the model and for HoMnO$_3$, φ_0 is ~144° [10]. As shown below, this distortion plays a crucial role in generating ferroelectricity in the E phase. The introduction of $\varphi_0 < 180°$ effectively reduces the symmetry of the Hamiltonian (8), although it is still invariant with respect to the inversion symmetry centers located at every Mn site. It is the E phase magnetic order that causes a spontaneous symmetry breaking and induces the FE polarization.
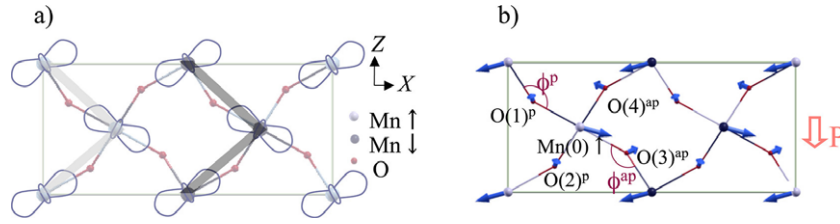
Figure 5. (a) Schematic representation of the spin and orbital ordering in the MnO_2 plane in AFM-E $HoMnO_3$. Zigzag chains are highlighted in gray and black. (b) Atomic displacements in FE $HoMnO_3$, as obtained by the difference of atomic coordinates in optimized AFM-E and optimized AFM-A spin configurations (length of arrows in arbitrary units). The relevant structural parameters are shown, as well as the direction of the ferroelectric polarization. Adapted from [34].

Since many results obtained with the model (8) regarding magnetic and orbital order were reported before in [19], in [13] we focused our attention on the new results directly related to the ferroelectricity of the E phase. A typical low temperature E phase MC snapshot is shown in figure 4(b). Since there is no spin–orbit interaction, the Hamiltonian (8) is invariant with respect to collective spin rotations; therefore the preferred spin direction is chosen randomly in our MC simulations. However, the ferromagnetic zigzag chains are clearly evident in the ground state. As observed from the snapshot, the double-exchange physics plays a crucial role in the formation of the FE state. The factor $C_{\mathbf{i},\mathbf{i}+\mathbf{a}}$ forbids electron hopping between Mn atoms with antiparallel t_{2g} spins. In this case, the displacement of the corresponding oxygen atom perpendicular to the Mn–Mn bond is only due to the elastic energy, which results in a Mn–O–Mn angle φ_0. On the other hand, hopping is allowed along the ferromagnetic zigzag chains[8]. In this case, the competition between the hopping energy (which is minimal for the 180° bond) and elastic energy will lead to a bond angle φ such that $\varphi_0 < \varphi < 180°$ (see figure 4(c)). Therefore, since φ only depends on the FM versus AFM nature of the bond, the direction of the oxygen displacements is the same in all zigzag chains, even though neighboring chains have opposite spin. This will lead to the coherent displacement of the center of mass of the O atoms with respect to the Mn sublattice, in a similar way to what is proposed in [4] for the field-induced phase of $TbMnO_3$. Figures 4(b) and (c) clearly show that the resulting FE polarization points along the diagonal connecting the next nearest neighboring Mn atoms, i.e. the orthorhombic a axis, in excellent agreement with Landau theory. This is a new mechanism for ferroelectricity in the E phase, and more theoretical and experimental work is needed to confirm its realization in $HoMnO_3$.

3. Predictions based on density functional theory

3.1. Technicalities: structural and computational details

In addition to the model Hamiltonian studies, *ab initio* computer simulations based on the generalized gradient approximation (GGA) [22] to density functional (DF) theory were performed. The results were extensively discussed in [23] and will be here summarized. Calculations were done using

---

[8] Although virtual hopping is allowed along the zigzag chains, the E phase is a band insulator [19].
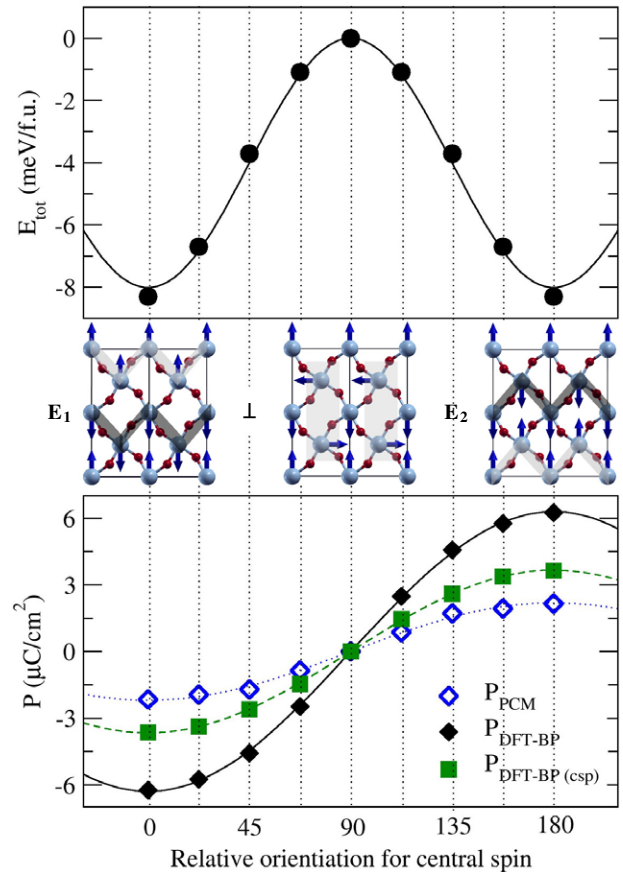

Figure 6. Upper panel: total energy as a function of the orientation of the central spins (see highlighted rectangles in the central $\perp$ spin configuration) with respect to the spin of the Mn in the origin (measured in degrees). Lower panel: polarization calculated via the PCM (empty diamonds) and quantum mechanically via DFT–BP (filled black diamonds). The squares denote the values obtained via the DFT–BP approach for centrosymmetric atomic configurations, as explained in the text. The lines are fits to $P \propto -\cos\phi$ with constant coefficients. Results reproduced from [23].

the Vienna *ab initio* simulation package (VASP) [24] and the projector augmented wave pseudopotentials [25]. We used a plane wave energy cut-off equal to 500 (400) eV for the collinear (non-collinear) calculations. The Brillouin zone was sampled with the $3 \times 4 \times 6$ shell [26]. The Berry phase approach [27, 28] was used to calculate P, integrating over six **k**-point strings parallel to the c axis, each string containing

six **k**-points. Non-collinear calculations were performed following [29]. Spin–orbit coupling (SOC) was neglected.

As for the construction of maximally localized Wannier functions (WFs) [30] we used the FLEUR code [31], an implementation of the full potential linearized augmented plane wave (FLAPW) approach [32]. Muffin-tin radii were set to 2.5, 2.0 and 1.5 au for R, Mn and O atoms, respectively, and the wavefunction cut-off was chosen as 3.8 au^{-1}. The Brillouin zone was sampled with 12 special **k**-points. The Wannier function calculation, whose procedure was recently implemented in the FLEUR code [33], was done with 512 **k**-points.

The magnetically induced polarization was evaluated by using three different approaches: (i) the point charge model (PCM) where each ion has been given its nominal valence (Ho: $+3$, Mn: $+3$, O: -2); (ii) the Berry phase (BP) method, and (iii) the Wannier function (WF) method. Remember that, in the first approach only the positions of the anions and cations are considered, whereas in the two latter [27, 28] quantum mechanical treatments, the self-consistent electronic structure is fully taken into account.

As for the structural details, we chose the experimental lattice constants [9] for HoMnO$_3$ for the orthorhombic unit cell (*Pnma* setting, $a = 5.835$ Å, $b = 7.361$ Å and $c = 5.257$ Å) and performed atomic relaxations until the Hellmann–Feynman forces were below 0.015 eV Å^{-1}.

3.2. Polarization estimate for AFM-E HoMnO$_3$ and magnetoelectric switching

In order to discuss FE in the system, let us start with the discussion of the *ab initio* calculated pattern of atomic displacements (cf figure 5(b)) in the non-centrosymmetric AFM-E spin configuration with respect to the inversion symmetric AFM-A structure[9]. The Mn atoms displace in total by 0.04 Å with respect to the initial centrosymmetric *Pnma* structure; however, the a and b displacement components of different Mn atoms compensate each other, whereas the c components add up to a net displacement of 0.01 Å per Mn atom along the negative direction of the c axis. Similarly, the in-plane O atoms are displaced by about 0.02 Å with the resulting c axis displacement of 0.01 Å per atom in the positive direction. Interplane O and Ho atoms contribute in a weaker way to ferroelectricity, so the total polarization along the c direction is estimated as $P_{\mathrm{PCM}} = -2.09 \ \mu$C cm^{-2}. Therefore, our optimized positions (within a bare ionic model for the P evaluation) confirm the large electric polarization suggested by means of modeling in the previous section [13].

In order to perform a fully quantum mechanical analysis of the polarization (including ionic and electronic contributions) [23], we considered a FE–AFM switching path from the two different domains E1 and E2, supposed to give $-P$ and $+P$ [13], via progressive rotation of the central spins (cf the insets in figure 6). The calculated

total energy of the system as a function of the spin rotation (cf figure 6 upper panel) clearly shows a double-well structure, an incontrovertible indication of the ferroelectric stabilization. Therefore, a mechanism for FE switching through a 180° rotation of Mn spins is put forward to accomplish the long-sought electrical control of AFM domains. Moreover, we report in figure 6 lower panel the polarization (evaluated both via the point charge model (PCM, i.e. using nominal ionic valences) and the Berry phase (BP) approach within the density functional theory (DFT–BP)) along the previously mentioned AFM/FE switching path. In agreement with a basic displacement-like mechanism for ferroelectricity, P switches from negative (in E1) to positive (in E2) and vanishes when the relative orientation of the central spins with respect to the other fixed spins is 90° (the spin configuration denoted as '$\perp$' in figure 6, which, due to the equivalence of all the O, shows centrosymmetric positions and zero BP term). The progressive distortions, responsible for ferroelectricity, in going from the $\perp$ to the collinear E phase are shown in figure 7, in terms of Mn–O–Mn angle and Mn–O bond lengths. Along the FE–AFM switching path, it is evident that the O atoms become progressively more inequivalent, as shown by the Mn–O–Mn angle between FM spins which becomes clearly larger (by about 3°) than that for the AFM coupled Mn spins. In parallel, the Mn–O 'long' bond lengths also become inequivalent.

As for the value of polarization, remarkably the calculated P of 6 μC cm^{-2} (cf figure 6) is the largest 'magnetically induced' P so far observed in the whole class of IMFs. The large difference between the PCM and the DFT–BP approach suggests that purely electronic effects are relevant for the final P. To clarify this issue, we estimated P considering the atomic centrosymmetric positions of the '$\perp$' structure and we artificially switched progressively the AFM-E1 or the AFM-E2 spin configurations, keeping the internal degrees of freedom fixed (i.e. no atomic relaxation allowed). As a result, in this latter case, due to structural centrosymmetry, there is no contribution from atomic displacements. However, the calculated DFT–BP polarization is found to be up to 3 μC cm^{-2} (see the green symbols in figure 6(b)). Remarkably, this is one of the first examples of a large contribution to P having an 'electronic' origin and deriving from the breaking of inversion symmetry by the AFM-E ordering, in addition to being one of the first *ab initio* studies focused on magnetically triggered improper ferroelectricity.

3.3. Wannier function analysis and microscopic mechanism for ferroelectricity

WFs represent an extremely useful tool in various contexts: on one hand, they provide a real space picture of the system's relevant polar orbital states; on the other side, the WF formalism allows the separation of the total P into contributions coming from different sets of orbitals and related WFs.

For clarity, we show in figure 8 the AFM-E HoMnO$_3$ insulating density of states (DOS) where the relevant states are highlighted: Mn e_g, Mn t_{2g}, and O p orbitals. These three sets of occupied eigenstates have been separately projected

---

[9] In our previous calculations [23], our reference PE structure was different from AFM-A chosen here and showed some non-collinear spin arrangements. However, the different path does not affect the final results as far as the polarization is concerned.
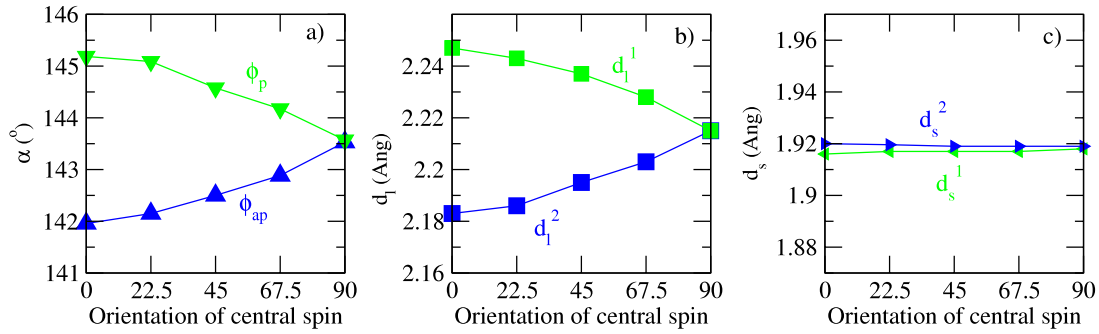
Figure 7. Structural parameters in going from the *E* phase (left x-axis, i.e. collinear spin arrangements between Mn at the origin and Mn in the central region) to the ⊥ structure (right x-axis, i.e. perpendicular spin arrangements between Mn in the origin and Mn in the central region): (a) Mn–O–Mn angles (in degrees) for parallel spins (down-triangles) and antiparallel spins (up-triangles). ((b), (c)) Two inequivalent Mn–O 'long' and 'short' in-plane bond lengths, respectively (in Å).

Table 1. WFC displacements with respect to the ion positions in AFM-E HoMnO$_3$ (Å). Only the up spin contribution is reported. Orbitals are denoted in a local frame (x: medium, y: short, z: long axis. Adapted from [34].

		ΔX	ΔY	ΔZ	$|\mathrm{d}r|$
Mn(0)	e_g: z^2	−0.169	0.044	0.188	0.257
	t_{2g}: xy	0.021	−0.008	−0.017	0.028
	t_{2g}: yz	−0.049	0.018	−0.146	0.155
	t_{2g}: zx	0.013	0.007	−0.008	0.016
O(1)^p	p_x	−0.158	0.071	0.200	0.265
	p_y	−0.110	0.048	0.209	0.241
	p_z	0.004	0.037	0.108	0.115
O(3)^{ap}	p_x	0.020	−0.001	−0.026	0.033
	p_y	−0.025	−0.013	−0.038	0.047
	p_z	−0.171	−0.016	0.048	0.178

Figure 8. DOS for the AFM-E phase of HoMnO$_3$ in the FE state: (a) total DOS, (b) Mn orbitally resolved DOS, (c) O^p (bold solid) and O^{ap} (thin dashed) projected DOS. Units on the *y* axis are states eV^{-1} per unit cell (a) or per atom ((b), (c)).

on a real space basis and 'maximally localized' to obtain the corresponding WFs. The contribution from deeper occupied valence states (such as O 2s and R 5s, 5p states) has been neglected. Within the WF formalism, the total polarization is evaluated as the sum of the displacements of the centers of each WF from the position of each related ion, added to the PCM polarization. According to the WF, our estimated value for the polarization in AFM-E HoMnO$_3$ [34] is $P_{WF} = -5.6 \ \mu C \ cm^{-2}$, to be compared with the value reported above from the Berry phase formalism, $P_{BP} = -6.1 \ \mu C \ cm^{-2}$, and from the bare ionic model, $P_{PCM} = -2.1 \ \mu C \ cm^{-2}$. The difference between polarization P_{WF} (P_{BP}) and P_{PCM} is often indicated as the *anomalous contribution* [35] and it is here discussed in terms of Wannier functions. In table 1, we show the orbitally decomposed polarization obtained by the displacement of the center of the WF (WFC) with respect to ionic positions for each set of bands: from the z components, one can see which are the main contributions to the final P.

Let us first consider the e_g-like d$_{z^2}$ and d$_{yz}$ orbitals which, along with O p orbitals, give the strongest contribution to the polarization (see the main displacements along the polar c axis in table 1). In figure 9(a), we show the WF for the e_g orbital at the Mn(0) up site surrounded by four O ions and four second-neighbor Mn ions in the ac plane. Due to orbital ordering, the e_g: d$_{z^2}$ orbital of the Mn(0) ion is elongated in the direction of the two O ions along the 'long' bond (which
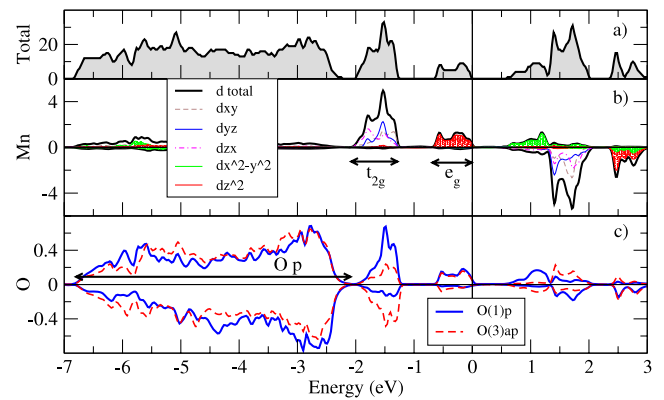
we define as z in a 'local' octahedron frame). Therefore, it forms a σ bonding with the O(1)^p and O(3)^{ap} p_z orbitals. In addition, when considering the AFM-E spin configuration, the up spin electron of the e_g orbital of the Mn(0) ion can hop only onto the Mn(1) (up spin) site via the O(1)^p atom and not on Mn(3) (which shows a down spin). This *asymmetric* hopping is responsible for giving a very large deviation of the WFC from the Mn ionic position (up to 0.26 Å; see the green arrow in figure 9(a)). Furthermore, recall that the hopping energies favor a larger Mn–O–Mn angle ϕ. As a consequence, in order to increase the hopping, the Mn(0) ion is expected to move toward O(3)^{ap} to increase ϕ^p between parallel Mn spins, i.e. along a direction which is opposite to the WFC displacement. With the same aim of increasing the hopping amplitude, O(1)^p moves perpendicularly to the Mn$^\uparrow$–Mn$^\uparrow$ bonding. Similarly, the O(3)^{ap} atom is displaced perpendicularly to the Mn$^\uparrow$–Mn$^\downarrow$ bonding. This explains what is shown in figure 5(b), showing the ions displacing in order to enhance the polarization as induced by the asymmetric hopping of e_g orbital electrons. Moreover, the displacement of the Mn ion (cf figure 5(b)) causes a current whose direction coincides with the current from the electron hopping and, therefore, it strengthens the net electronic polarization. It should be noted
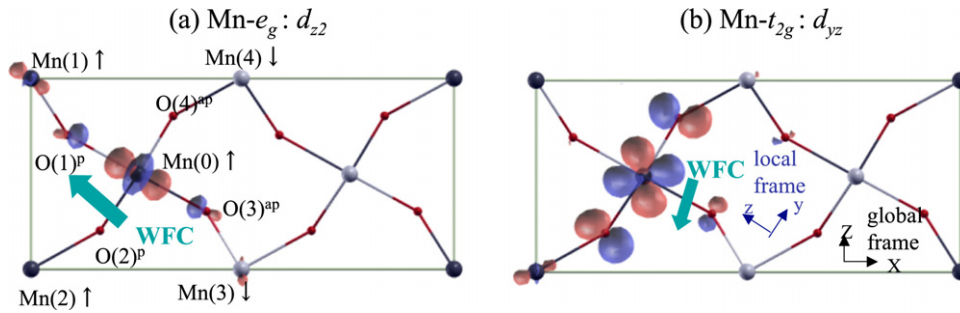
Figure 9. Isosurface of WFs for Mn d states centered on Mn(0) in AFM-E HoMnO$_3$: (a) e$_g$ and (b) t$_{2g}$ states. Arrows indicate the displacement of WFCs from the Mn atomic position. Here, the superscript p (ap) of O denotes the oxygen ion between the parallel (antiparallel) spins of the Mn ions. Adapted from [34].

that the atomic displacement (0.04 Å) is much smaller than the displacement of the WF center (0.26 Å). Therefore, at variance with the conventional mechanism of polarization in standard ferroelectrics [35] where polarization is driven by atomic displacements, here the mechanism is 'magnetically driven' and the atomic displacement appears as a 'secondary' effect occurring mainly to enhance the asymmetric hopping integrals.

Let us now discuss what happens for the t$_{2g}$: d$_{yz}$ orbital which forms a π-like bonding with the surrounding O p states. Because of its planar isotropic symmetry, the degree of hybridization of the d$_{yz}$ orbital with the O p state mainly depends on the bond distance. Figure 9(b) shows that the d$_{yz}$ orbital hybridizes with O(2)^p p$_z$ and O(4)^{ap} p$_z$. As already pointed out for the e$_g$ orbital case, the electron hops only into the Mn(2) up site, so the WFC is displaced in that direction (see the green arrow in figure 9(b)). Moreover, the atomic displacement induced by the e$_g$ orbital—explained above—causes a shorter bond length between the Mn(0) and O(3)^{ap} ions (see weight of the Mn t$_{2g}$ WF on O(3)^{ap}); as a consequence, the increased hybridization slightly changes the direction of the WFC displacement with respect to the Mn(0)– Mn(2) direction. Therefore, in HoMnO$_3$, the anomalous contributions from Mn e$_g$ and t$_{2g}$ orbitals almost cancel each other along the polar c direction, with the O p states therefore giving the main contribution (cf table 1).

4. Conclusions

The multiferroic behavior of distorted rare-earth manganites was here briefly reviewed. The focus was on recent work by the authors using Hamiltonian modeling and density functional approaches. The readers can find more details and references in the original publications of our group.

The Dzyaloshinskii–Moriya interaction was invoked as a possible natural explanation for the coexistence of ferroelectricity and incommensurate magnetic phases. Its competition with double exchange and superexchange in a nearest neighbor model can lead to the stabilization of an ICM– FE phase; moreover, it inherently gives an explanation for the observed perpendicular directions of the polarization and modulation vectors in the several spiral magnetic multiferroics discovered so far.

Using modeling calculations, another mechanism, independent of the spin–orbit coupling, was proposed for manganites in the AFM-E phase. This mechanism is based on the interplay between electron hopping and elastic energy in distorted perovskites, and it can lead to ferroelectricity with a sizable polarization. Indeed, the latter is confirmed by means of first-principles calculations performed on ortho-HoMnO$_3$, from which the estimated polarization is up to 6 μC cm^{-2}, the largest reported so far for magnetically induced ferroelectricity. In addition, the nature of the polarization is found to be 'dual', arising in part from conventional atomic displacements and in part from a purely electronic source. Although HoMnO$_3$ was considered here as a test case, we believe that our findings on the dual nature of ferroelectricity—as arising from a symmetry breaking induced by the magnetic order—have a wider range of validity for the family of improper magnetic FEs, where both the lattice and electronic degrees of freedom should be taken into account accurately since they are simultaneously relevant.

References

[1] Mostovoy M and Cheong S W 2007 *Nat. Mater.* **6** 13
[2] Ramesh R and Spaldin N A 2007 *Nat. Mater.* **6** 21
[3] Kenzelmann M *et al* 2005 *Phys. Rev. Lett.* **95** 087206
[4] Aliouane N *et al* 2006 *Phys. Rev.* B **73** 020102(R)
[5] Kimura T, Goto T, Shintani H, Ishizaka K, Arima T and Tokura Y 2003 *Nature* **426** 55
[6] Hur N, Park S, Sharma P A, Ahn J S, Guha S and Cheong S W 2004 *Nature* **429** 392
[7] Goto T, Kimura T, Lawes G, Ramirez A P and Tokura Y 2004 *Phys. Rev. Lett.* **92** 257201
[8] Kimura T, Lawes G, Goto T, Tokura Y and Ramirez A P 2005 *Phys. Rev.* B **71** 224425

[9] Alonso A J, Martinez-Lope M J, Casais M T and Fernandez-Diaz M T 2000 *Inorg. Chem.* **39** 917
[10] Kimura T, Ishihara S, Shintani H, Arima T, Takahashi K T, Ishizaka K and Tokura Y 2003 *Phys. Rev.* B **68** 060403(R)
[11] Picozzi S, Yamauchi K, Bihlmayer G and Bluegel S 2006 *Phys. Rev.* B **74** 094402
[12] Lorenz B, Wang Y Q and Chu C W 2007 *Phys. Rev.* B **76** 104405
[13] Sergienko I A, Sen C and Dagotto E 2006 *Phys. Rev. Lett.* **97** 227204
[14] Sergienko I A and Dagotto E 2006 *Phys. Rev.* B **73** 094434
[15] Blasco J *et al* 2000 *Phys. Rev.* B **62** 5609
[16] Dzyaloshinsky I 1958 *J. Phys. Chem. Solids* **4** 241
[17] Moriya T 1960 *Phys. Rev.* **120** 91
[18] Dagotto E, Hotta T and Moreo A 2001 *Phys. Rep.* **344** 1
[19] Hotta T *et al* 2003 *Phys. Rev. Lett.* **90** 247203
[20] Efremov D V, van den Brink J and Khomskii D I 2004 *Nat. Mater.* **3** 853
[21] Slater J C and Koster G F 1954 *Phys. Rev.* **94** 1498
[22] Perdew J P, Burke K and Ernzerhof M 1996 *Phys. Rev. Lett.* **77** 3865

[23] Picozzi S, Yamauchi K, Sanyal B, Sergienko I A and Dagotto E 2007 *Phys. Rev. Lett.* **99** 227201
[24] Kresse and Furthmüller J 1996 *Phys. Rev.* B **54** 11169
[25] Kresse G and Joubert G 1999 *Phys. Rev.* B **59** 1758
[26] Monkhorst H J and Pack J D 1976 *Phys. Rev.* B **13** 5188
[27] King-Smith R D and Vanderbilt D 1993 *Phys. Rev.* B **47** 1651
[28] Resta R 1994 *Rev. Mod. Phys.* **66** 899
[29] Hobbs D, Kresse G and Hafner J 2000 *Phys. Rev.* B **62** 11556
[30] Marzari N and Vanderbilt D 2001 *Phys. Rev.* B **56** 12847
[31] http://www.flapw.de
[32] Wimmer E, Krakauer H, Weinert M and Freeman A J 1981 *Phys. Rev.* B **24** 864
[33] Freimuth F, Mokrousov Y, Wortmann D, Heinze S and Blügel S 2008 unpublished
[34] Yamauchi K, Freimuth F, Blügel S and Picozzi S 2008 *Preprint* 0803.1166
[35] Ghosez Ph, Michenaud J P and Gonze X 1998 *Phys. Rev.* B **58** 6224
[36] Kubo K 1982 *J. Phys. Soc. Japan* **51** 782
[37] Dagotto E *et al* 1998 *Phys. Rev.* B **58** 6414